The Journal of Experimental Biology 209, 3558-3568
Published by The Company of Biologists 2006
doi:10.1242/jeb.02469

Effective elastic modulus of isolated gecko setal arrays

K. Autumn[1,*], C. Majidi[2], R. E. Groff[2,†], A. Dittmore[1] and R. Fearing[2]

[1]*Department of Biology, Lewis & Clark College, Portland, OR 97219, USA and* [2]*Department of Electrical Engineering and Computer Science, University of California, Berkeley, CA 94720, USA*

*Author for correspondence (e-mail: autumn@lclark.edu)

†Present address: Dept of Electrical and Computer Engineering, Clemson University, Clemson, SC 29634, USA

Accepted 5 June 2006

Summary

Conventional pressure sensitive adhesives (PSAs) are fabricated from soft viscoelastic materials that satisfy Dahlquist's criterion for tack with a Young's modulus (*E*) of 100 kPa or less at room temperature and 1 Hz. In contrast, the adhesive on the toes of geckos is made of β-keratin, a stiff material with *E* at least four orders of magnitude greater than the upper limit of Dahlquist's criterion. Therefore, one would not expect a β-keratin structure to function as a PSA by deforming readily to make intimate molecular contact with a variety of surface profiles. However, since the gecko adhesive is a microstructure in the form of an array of millions of high aspect ratio shafts (setae), the effective elastic modulus (E_{eff}) is much lower than *E* of bulk β-keratin. In the first test of the E_{eff} of a gecko setal adhesive, we measured the forces resulting from deformation of isolated arrays of tokay gecko (*Gekko gecko*) setae during vertical compression, and during tangential compression at angles of +45° and –45°. We tested the hypothesis that E_{eff} of gecko setae falls within Dahlquist's criterion for tack, and evaluated the validity of a model of setae as cantilever beams. Highly linear forces of deformation under all compression conditions support the cantilever model. E_{eff} of setal arrays during vertical and +45° compression (along the natural path of drag of the setae) were 83±4.0 kPa and 86±4.4 kPa (means ± s.e.m.), respectively. Consistent with the predictions of the cantilever model, setae became significantly stiffer when compressed against the natural path of drag: E_{eff} during –45° compression was 110±4.7 kPa. Unlike synthetic PSAs, setal arrays act as Hookean elastic solids; setal arrays function as a bed of springs with a directional stiffness, assisting alignment of the adhesive spatular tips with the contact surface during shear loading.

Key words: gecko, adhesion, pressure sensitive adhesive, material science, contact mechanics, biomechanics.

Introduction

Gecko toe pads (Fig. 1A,B) are sticky because they feature an extraordinary hierarchy of structure (Fig. 2) that functions as a smart adhesive (Autumn, 2006; Fakley, 2001). The gecko adhesive is a microstructure in the form of an array of millions of high aspect ratio shafts (Fig. 1C). A single seta of the tokay gecko is approximately 110 μm in length and 4.2 μm in diameter (Ruibal and Ernst, 1965; Russell, 1975; Williams and Peterson, 1982) (Fig. 1D). Setae are similarly oriented and uniformly distributed on the scansors. Setae branch at the tips into 100–1000 more structures (Ruibal and Ernst, 1965; Schleich and Kästle, 1986), known as spatulae (Fig. 1E), which make intimate contact with the surface. Structurally, the adhesive on gecko toes differs dramatically from that of conventional adhesives. Gecko setae are formed from β-keratin (Russell, 1986; Wainwright et al., 1982), a material orders of magnitude stiffer than those used to fabricate pressure sensitive adhesives (PSAs). Conventional PSAs, such as those used in adhesive tapes, must be sufficiently soft and sticky to flow and make intimate and continuous surface contact. PSAs are fabricated from soft viscoelastic materials that satisfy Dahlquist's criterion for tack with a Young's modulus, *E*, of 100 kPa or less at room temperature and 1 Hz (Dahlquist, 1969; Pocius, 2002). Because they are soft and sticky, PSAs also tend to degrade, foul, self-adhere, and attach accidentally to inappropriate surfaces.

The effective elastic modulus of a gecko setal array, E_{eff} (Persson, 2003; Sitti and Fearing, 2003), is likely to be much lower than *E* of bulk β-keratin; arrays of setae should behave as a softer material than bulk β-keratin. Young's modulus of β-keratin in tension is approx. 2.5 GPa in bird feathers (Bonser and Purslow, 1995) and 1.3–1.8 GPa in bird claws (Bonser, 2000). Young's moduli of lizard beta keratins in general (Fraser and Parry, 1996), and gecko beta keratins in particular (Alibardi, 2003; Russell, 1986; Wainwright et al., 1982), remain unknown at present, but can be assumed to be in the neighborhood of 1–3 GPa. The behavior of a setal array during compression and relaxation will

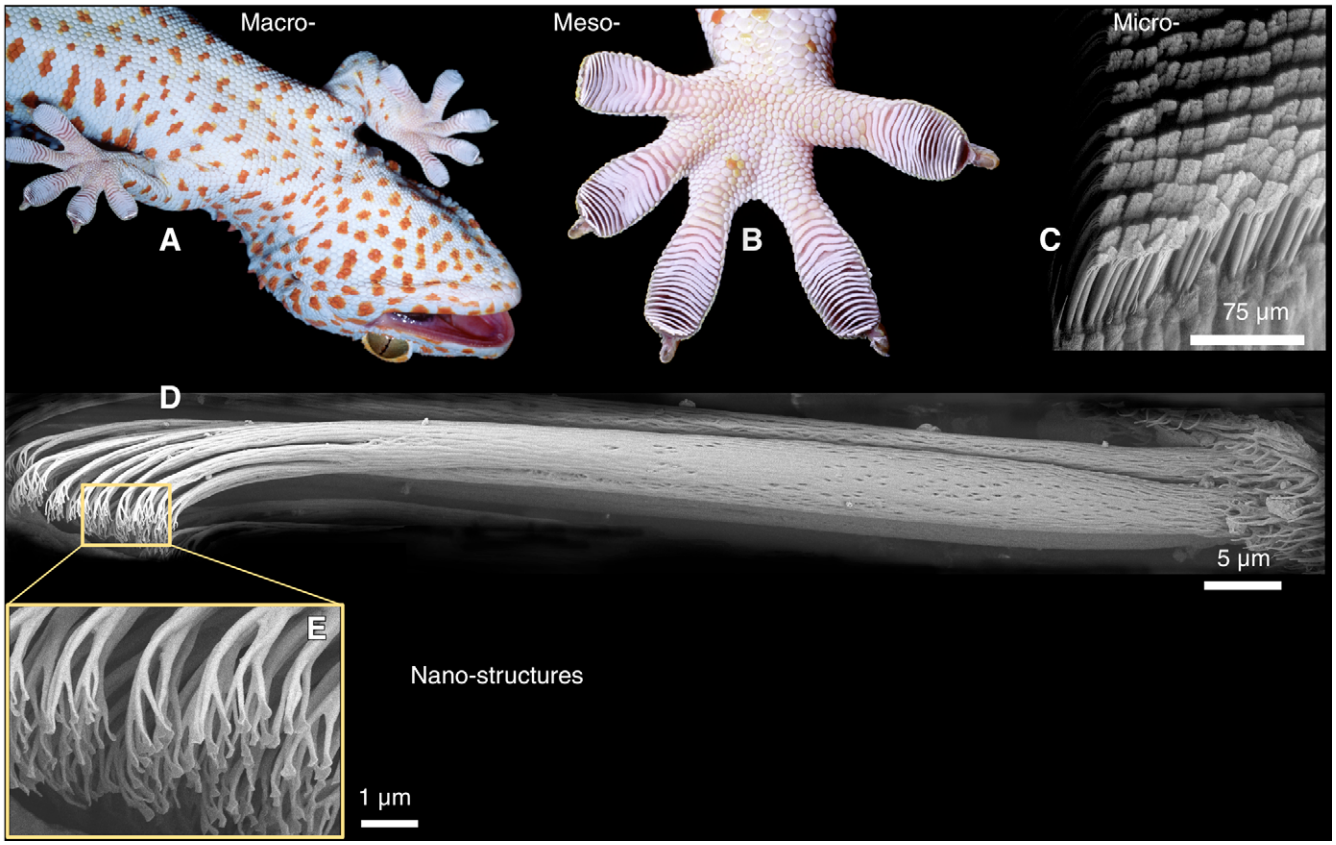

Fig. 1. Structural hierarchy of the gecko adhesive system.

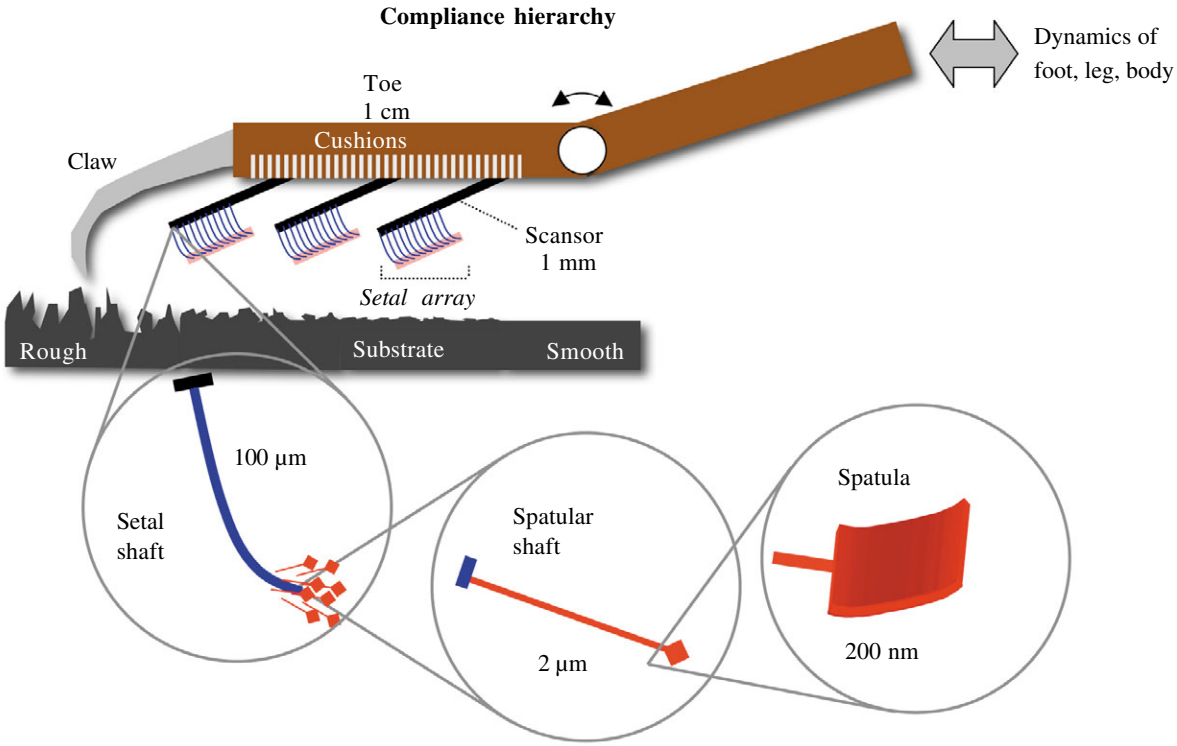

Fig. 2. Schematic of compliance hierarchy of the gecko adhesive system (for reviews, see Autumn, 2006; Russell, 2002).

depend on the mode(s) of deformation of individual setae. Bending is a likely mode of deformation of setae (Simmermacher, 1884), and a simple approach is to model arrays of setae as cantilever beams (Autumn, 2006; Glassmaker et al., 2004; Hui et al., 2004; Persson, 2003; Sitti and Fearing, 2003; Spolenak et al., 2005). An alternative approach is that of column buckling (Jagota and Bennison, 2002), a model that has also been used to study the effective modulus of an array of vertical multi-walled carbon nanotubes (Tong et al., 2005).

Cantilever model

Current studies of setal deformation generally treat a single seta as a cylindrical elastic rod of radius R with a modulus of elasticity E and area moment of inertia $I=\pi R^4/4$. When a load F is applied to the tip of the rod in the direction perpendicular to the supporting substrate, the rod will deform and the tip will displace by an amount Δ in the same direction.

If the rod is naturally perpendicular to the substrate, then Δ is only significant after a critical buckling load is exceeded. For this special case, the seta is represented by a column buckling model (Jagota and Bennison, 2002). Microscopic images of the setal array, however, show that setae are naturally deflected from the perpendicular axis. Let the angle ϕ denote the natural (undeformed) slope of the seta with respect to the surface of the supporting substrate. When ϕ is less than 90°, a more general theory is used to study setal deformation. The elastica model (Frisch-Fay, 1962) predicts the shape of a cantilevered elastic rod subjected to a load at the tip with a specified angle. The model is a second order boundary value problem, which for the present case has a concise solution for tip deflection Δ as a function of load F:

$$\Delta = L\sin(\phi) - [F(p,m) - F(p,n) + 2E(p,n) - 2E(p,m)] / k , \quad (1)$$

where $F(\bullet,\bullet)$ and $E(\bullet,\bullet)$ are the elliptic integrals of the first and second kind, respectively, $n=\pi/2$, $k=(F/EI)^{1/2}$, $m=\arcsin(\sin(\pi/4-\phi/2)/p)$, and the modulus p is the solution to:

$$kL = F(p,n) - F(p,m) . \quad (2)$$

The modulus p is determined numerically over the domain $\sin(\pi/4-\phi/2)$ to $\sin(3\pi/4-\phi/2)$ by solving Eqn 2 with a nonlinear equation solver in Matlab 7 (The Mathworks Inc., Natick, MA, USA). Substituting the solution for p into Eqn 1 yields a relationship between the applied load F and the resulting tip displacement Δ. Plots of F *vs* Δ for values of ϕ ranging from 30 to 90° are given in Fig. 3A.

Following arguments (Frisch-Fay, 1962), Eqn 1 can be modified to admit an additional shear load V that acts on the tip in the direction parallel to the surface of the supporting substrate. This force is generated when the setal array is dragged along the surface during compressive loading. The magnitude is limited by Coulomb friction (Bhushan, 2002) and so in general:

$$|V| = \mu F + S , \quad (3)$$

where the friction coefficient μ is typically 0.25 for polymeric surfaces, and where S is the shear strength due to interfacial adhesion. Since measurements are performed on a Teflon™ substrate with relatively large compressive loads, the contribution of adhesion to the shear force is negligible and so Eqn 3 is assumed to reduce to $|V|=\mu F$.

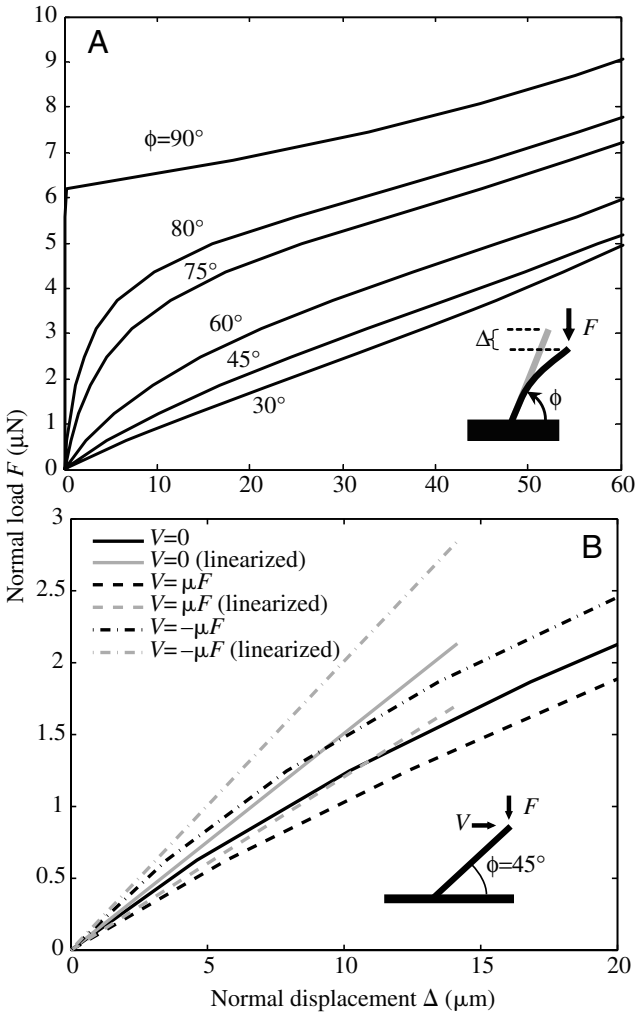

Fig. 3. (A) Force–displacement relationship of an elastic rod for L=100 μm, R=2 μm, and E=2 GPa. As ϕ increases, the behavior transitions from cantilever bending to column buckling. (B) Normal force–displacement relationship of the full elastica model (black) and small-deflection, linearized approximation (gray) under differing shear loads for an elastic rod with L=100 μm, R=2 μm, E=2 GPa, ϕ=45°, and μ=0.25.

Interestingly, for a rod with a natural deflection of 45° ($\phi<\pi/4$), elastic rod theory predicts that under a combined loading F and $V=\mu F$, the rod becomes more compliant for low F. If, however, the rod is dragged against its natural orientation (i.e. $V=-\mu F$), it becomes stiffer. This can be seen more simply by examining the linearized approximation to elastica.

For a naturally angled seta, Eqn 1 may be simplified by assuming that deformation is governed by small-deflection cantilever bending. In this cantilever bending approximation, loads parallel to the beam cause no deflection and loads transverse to the beam cause a transverse deflection governed

by spring constant $3EI/L^3$. Finding the transverse components of F and $V=\pm\mu F$, and computing the normal component of the resulting deflection yields the following relationship between tip forces and the normal displacement (Campolo et al., 2003; Sitti and Fearing, 2003),

$$\begin{aligned}\Delta_{\text{approx}} &= \frac{L^3}{3EI}\left[F\cos^2(\phi) + V\sin(\phi)\cos(\phi)\right] \\ &= \frac{L^3}{3EI}\cos^2(\phi)\left[1 \pm \mu\tan(\phi)\right]F\,.\end{aligned} \tag{4}$$

As illustrated in Fig. 3B, this simple model predicts the same trend as elastica: higher stiffness when $V=-\mu F$ (sliding against the hair), intermediate stiffness when $V=0$ (no sliding), and lower stiffness when $V=\mu F$ (sliding with the hair).

Next, to derive an effective elastic modulus (E_{eff}) for a model setal array, we use Hooke's law,

$$\sigma = E_{\text{eff}}\epsilon\,, \tag{5}$$

where σ is the stress applied to the setal array and ϵ is the resulting strain, both along the perpendicular axis. For a setal density D, which has units of inverse area, the stress may be represented as,

$$\sigma = FD\,. \tag{6}$$

The resulting strain is defined as $\epsilon=\Delta/(L\sin\phi)$. Substituting Δ_{approx} for Δ yields:

$$\epsilon = \frac{L^2\cos^2(\phi)}{3EI\sin(\phi)}\left[1 \pm \mu\tan(\phi)\right]F\,. \tag{7}$$

Lastly, substituting the expressions for σ and ϵ given in Eqn 6 and Eqn 7 into Eqn 5 and solving for E_{eff} gives:

$$E_{\text{eff}} = \frac{3EID\sin(\phi)}{L^2\cos^2(\phi)\left[1 \pm \mu\tan(\phi)\right]}\,. \tag{8}$$

We now calculate the shaft angle ϕ required to yield an effective stiffness of 100 kPa (the upper limit of Dahlquist's criterion) (Dahlquist, 1969; Pocius, 2002). A typical tokay setal array has approx. 14 000 setae mm^{-2} (Schleich and Kästle, 1986) and $D=1.44\times10^{10}$ m^{-2}. Using Eqn 3, a value of $\phi=50°$ is required for $E=1$ GPa, and $\phi=36.65°$ for $E=2$ GPa to yield $E_{\text{eff}}=100$ kPa.

A template is the simplest model (fewest number of variables and parameters) that exhibits a targeted behavior (Full and Koditschek, 1999). This study focuses on evaluating the validity of the cantilever model as a template for setal deformation. We measured the forces associated with deformation of gecko setal arrays to test the hypotheses that (1) forces of deformation are an approximately linear function over the working range of displacements, as predicted by the cantilever model; (2) E_{eff} is below 100 kPa, as predicted by the Dahlquist criterion, and (3) stiffness is greater when the angle of deformation is negative (against the natural path of drag) than during vertical or positive angle deformations.

Materials and methods

Specimen preparation

Tokay gecko *Gekko gecko* L. setal arrays were peeled from seven live adult animals using the methods described (Hansen and Autumn, 2005). Test specimens were created by mounting the setal arrays on scanning electron microscope (SEM) stubs (product number 16261, Ted Pella, Redding, CA, USA) with cyanoacrylate adhesive (Loctite 410; Henkel Loctite Corp., Rocky Hill, CT, USA). 26 array specimens were examined in the study. Measurements were made from 2 h to 3 weeks following harvesting. We also examined five setal arrays taken from two individuals that had been stored at room temperature for approx. 2 years following harvesting.

Mechanical testing apparatus

Setal array specimens were mounted on SEM stubs and evaluated with a custom 2-axis mechanical tester (Fig. 4). The specimen chuck was attached to a Kistler 9328A 3-axis force sensor (Kistler, Winterthur, Switzerland) that was moved in the Z (up-and-down) and Y (left-and-right) axes with Newport 460P stages (Newport, Irvine, CA, USA) driven by closed loop brushless DC servomotors (Newport 850G-HS actuator in the Y axis and a Newport 850G actuator in the Z axis). The stage and force sensor assembly were vertically mounted to a stainless steel 'tombstone' above a Newport RP Reliance breadboard table. A Newport ESP 300 servocontroller drove the actuators. Force measurements were collected through an AD Instruments Maclab/4e data acquisition unit (ADInstruments, Milford, MA, USA). The stage controller and force acquisition were interfaced with a Powerbook G3 (Apple Computer, Cupertino, CA, USA) for automated control of array experiments. The stiffness of the 2-axis mechanical tester was measured by pressing a blank SEM stub into the breadboard table. The stiffness of the mechanical tester itself was about 320 N mm^{-1}. Pilot experiments showed that the setal arrays stiffness was in the range of 0.5–3 N mm^{-1}. Therefore, the primary compliant element in the test arrangement was the setal array itself. Test substrates are held in place by toggle strap clamps with spring plungers bolted to the Newport breadboard table. Array test specimens were mounted in the mechanical tester chuck so that their natural path of drag was in alignment with the Y axis. The array alignment was carried out with the help of a mirror. The compliant nature of the setal arrays allowed for small rotational misalignments without impacting the measurement of array physical properties.

The test substrate for the experiments was a 2 mm thick sheet of polytetrafluoroethylene (PTFE) that was washed with de-ionized water and dried with Kimwipes (Kimberly-Clark, Neenah, WI, USA) before each test sequence. We used three types of experiments to assess the stiffness of the array. Testing setal arrays along the natural path of drag ('along setal curvature') assesses their stiffness in the typical orientation that geckos use them to climb (Autumn et al., 2000; Ruibal and Ernst, 1965) (Fig. 5). Pressing the setal arrays against the natural path of drag ('against setal curvature') tests them

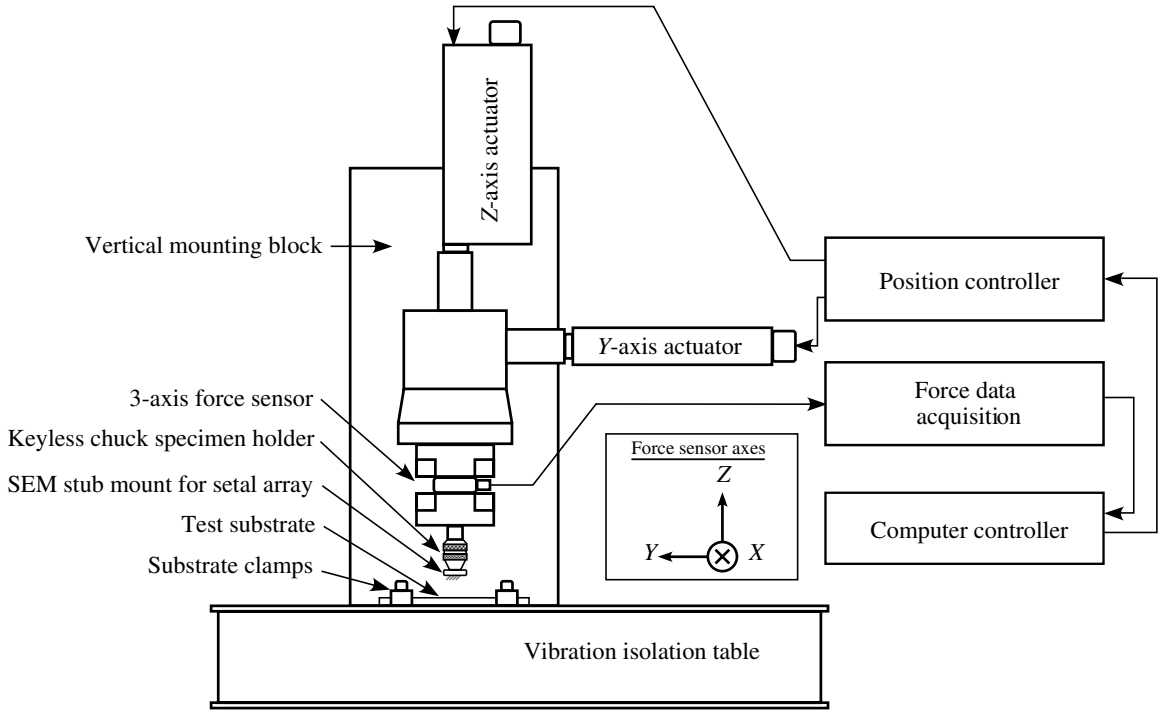

Fig. 4. Schematic of testing platform. A servocontroller drove two closed loop DC servomotors attached to a 2-axis linear stage to produce μm scale displacements of setal arrays bonded to SEM stubs. A 3-axis piezoelectric force sensor measured the forces associated with deformation of setal arrays compressed against a PTFE substrate.

opposite to the usual direction for climbing in which they do not adhere (Autumn et al., 2000). The straight up and down tapping test ('vertical') is the intermediate condition between these opposing directions. The stiffness tests were conducted with a crosshead speed of 50 μm s^{-1} in both the *Z* axis and the *Y* axis for all experiments, yielding compression frequency and relaxation frequency of approx. 1 Hz. Each array was tested with the three types of stiffness experiment in a symmetric design to control for repeated measures. Each experiment was conducted 10× per array (i.e. 30 measurements per array) to a compression level near its maximum. The straight up-and-down tap test did not include a drag portion whereas the 'along drag' and 'against drag' tests included a drag portion in the experiment. The short drag step in these tests allowed us to examine the effect of array orientation on coefficient of friction as well as array stiffness in a single experiment.

Setal array dimension

Estimation of the setal array modulus requires measurement of the array dimensions. After mounting arrays to SEM stubs, the specimens were inspected using a SMZ 1500 optical stereomicroscope (Nikon, Yokohama, Kanagawa, Japan) to ensure that the arrays were securely glued and the setae were free of glue that would interfere with the physical property measurements. Defective arrays were rejected from the study. Array area was measured by photographing each array under the optical microscope with 100 μm diameter stainless steel 'minutien' pins (Fine Science Tools, product number 26002-10, North Vancouver, BC, Canada) as a size reference. The digitized micrographs were examined with Canvas v. 9 (ACD, Saanichton, BC, Canada) drawing software to measure the area of each array.

After mechanical testing of the arrays, the stub-mounted specimens were prepared for SEM observation. Array

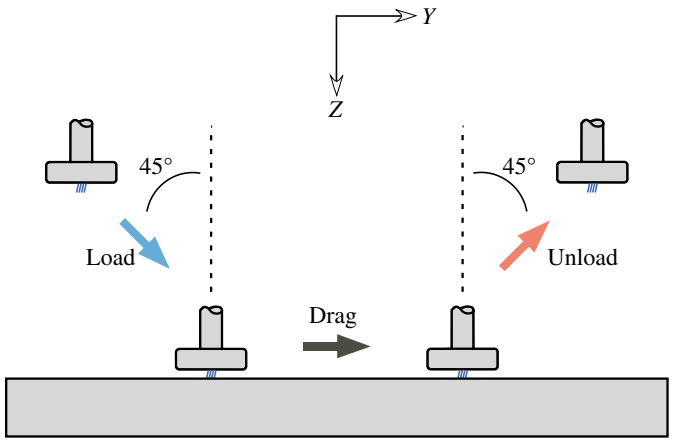

Fig. 5. Testing protocol for setal arrays deformed along the natural path of drag ('with setal curvature', in the typical orientation that geckos use them to climb. In this protocol, the 2-axis micropositioner approached the substrate at 45° until the array was compressed to approx. 50% of its resting height, moved 100 μm parallel to the substrate, and then retracted at –45°.

specimens were platinum–palladium sputter-coated using a Hummer VI plasma coater (Technics, Anatech Ltd, Denver, NC, USA). Each of the test specimens was then viewed in an Amray 1810 SEM (Amray, KLA-Tencor, Milpitas, CA, USA). Five photomicrographs were taken along the length of each array. The digitized photomicrographs were imported into Canvas 9 software for assessment of array height.

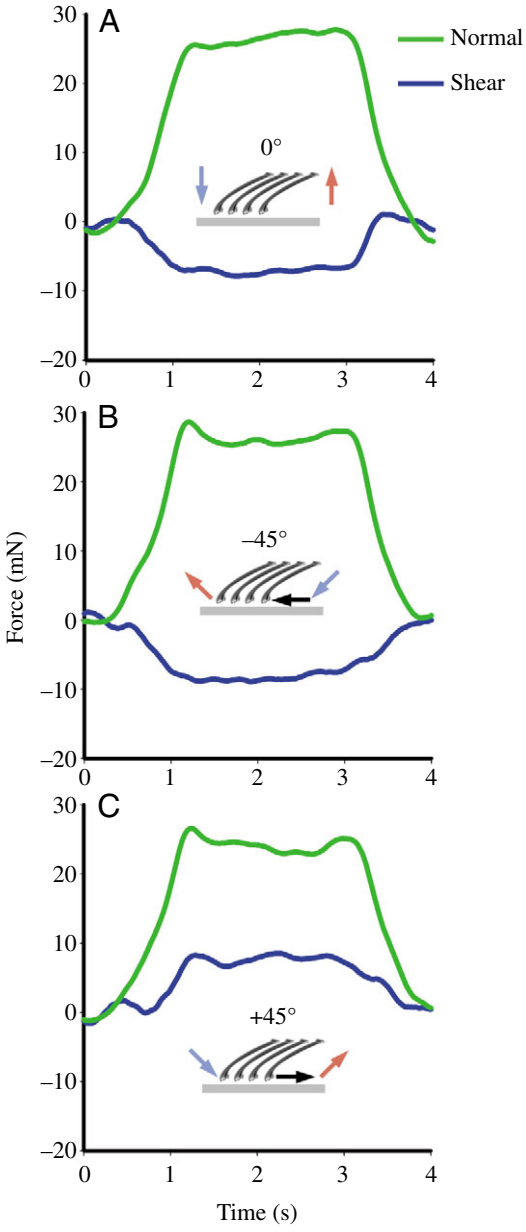

Fig. 6. Force *vs* time of representative trials. In all trials, shear velocity was 50 μm s^{-1}. (A) Setal arrays compressed and relaxed vertically. (B) Setal arrays compressed and relaxed against the natural path of drag ('against setal curvature'), opposite to the usual direction for climbing in which they do not adhere. (C) Setal arrays compressed and relaxed along the natural path of drag ('with setal curvature', in the typical orientation that geckos use them to climb.

Setal array stiffness

The raw force data were corrected for baseline drift of the sensor with a Mathematica (Wolfram Research, Champaign, IL, USA) program. Trials disrupted by mechanical vibrations were discarded. Slopes of loading and unloading curves were calculated using linear regression in Excel (Microsoft, Redmond, WA, USA), and then transformed to the physical properties of array stiffness (k_{array}), setal stiffness (k_{seta}), and array effective modulus (E_{eff}). For all plots of force (Figs 6, 7), raw data were filtered using a fast Fourier transform (FFT) kernel smoothing algorithm in SigmaPlot 9 (Systat Software, Inc., Point Richmond, CA, USA). The array stiffness, k_{array}, was taken directly from the compression loading and unloading curves. The array stiffness calculation treats the entire array as a single spring. We divided k_{array} by the number of setae on the array patch with area, A, and setal hair packing density, D, which for tokay geckos is 14 400 setae mm^{-2} (Autumn and Peattie, 2002; Schleich and Kästle, 1986):

$$k_{seta} = \frac{k_{array}}{A\,D} \quad . \tag{9}$$

The setal stiffness normalizes the data by array area. We then estimated the effective Young's modulus of a setal array, E_{eff}, by measuring the array height, L_0, and assuming the applied compression load is distributed evenly over the measured array area (i.e. a lower estimate of modulus). We used linear regression to evaluate the significance of linearity of the force–displacement curves, after trimming the period during initial preload. The statistically linear portion of the array tap data were modeled with Hookean elasticity where

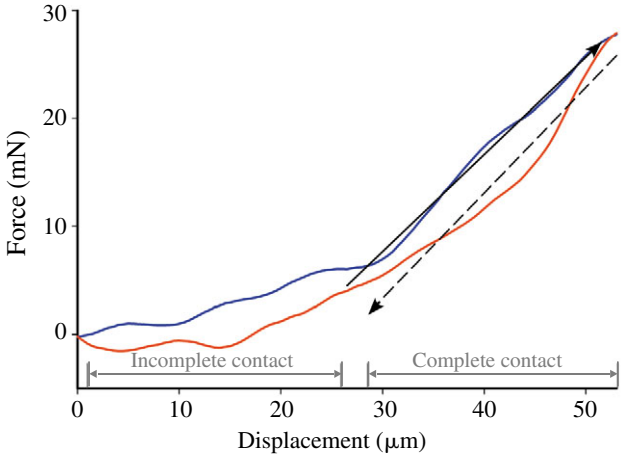

Fig. 7. Force *vs* displacement of setal array loaded and unloaded vertically. The initial section of the curve represents preloading of the array, before full contact with the test surface was made. Following preload, the forces of deformation were statistically linear for deformations up to approx. 50% of array height. Solid and broken arrows indicate linear fits for loading and unloading, respectively.

compression stress, σ, is a linear function of strain, ϵ, giving modulus as:

$$E_{\text{eff}} = \frac{\sigma}{\epsilon} \quad . \tag{10}$$

Now, the modulus can be expanded to:

$$E_{\text{eff}} = \frac{\sigma}{\epsilon} = \frac{F/A}{\Delta L/L_0} \quad , \tag{11}$$

where F is the applied load and ΔL is the change in array height in response to this force. If the setal array behaves as a Hookean spring and substituting

$$F = k_{\text{array}} \Delta L \tag{12}$$

into Eqn 11 gives the following expression for the effective modulus:

$$E_{\text{eff}} = \frac{k_{\text{array}} L_0}{A} \quad . \tag{13}$$

Setal array coefficient of friction

The coefficient of friction, μ, for the 'along drag' and 'against drag' conditions can be assessed since there is a sliding phase across the PTFE test substrate. The coefficient of friction is calculated as:

$$\mu_{\text{eff}} = \frac{|\text{Average } Y \text{ axis force}|}{\text{Average } Z \text{ axis force}} \quad . \tag{14}$$

Results

Setal array height and maximum compression

The tokay gecko array height averaged 68 μm (s.d.=17; 95% CI=65,71; N=155). Using a typical setal length of 100 μm, the average array height measurement of 68 μm yields an estimate of shaft angle of $\sin^{-1}(68/100)=43°$, consistent with observations using SEM. Maximum normal deflection during compression was approximately 50% of the array height. Maximum deflection averaged 33 μm for a 0° approach (s.d.=9; 95% CI=29,36; N=31) and 32 μm when the loading angle is 45° (s.d.=11; 95% CI=27,36; N=31).

Effective modulus and coefficient of friction

Forces of deformation during loading and unloading were statistically linear (P<0.0001) under +45°, vertical and –45° compression conditions (Fig. 6), supporting a model of beam bending and contradicting a model of buckling. E_{eff} of setal arrays during vertical and +45° compression were 83 kPa ± 4.0 se and 86 kPa ± 4.4 se respectively. Setae became significantly stiffer when compressed against the natural path of drag: E_{eff} during –45° compression was 110 kPa ± 4.7 se. Average array stiffness (k_{array}) and effective modulus (E_{eff}) differed by at most 10% between loading and unloading conditions (Figs 7, 8), and none of the differences was statistically significant (P>0.05). Mean (± s.e.m.) coefficient of friction (μ) during the drag step of the –45° trials was 0.244±0.007, and 0.29±0.01 during the drag step of the +45° trials.

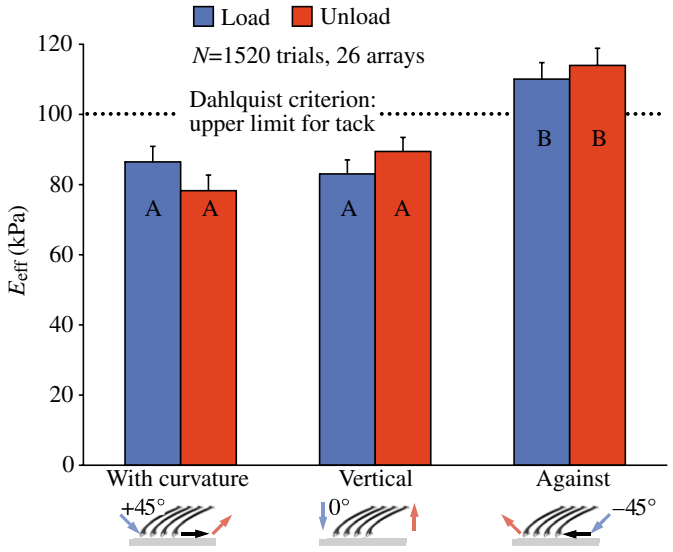

Fig. 8. Effective elastic modulus (E_{eff}) during deformation of isolated setal arrays. Horizontal labels denote direction of deformation relative to the curvature of the setae. Values are means ± s.e.m. Letters A,B denote significant ANOVA contrasts. Dotted line shows E_{eff}=100 kPa, the upper limit of Dahlquist's criterion for tack (Dahlquist, 1969; Pocius, 2002).

Effect of age of specimen

The age of the primary group of specimens (time after harvest) ranged from 2 h to 28 days. Over this time period, there was a subtle yet statistically significant (P<0.001) increase in stiffness over time after harvest. Linear regression revealed that arrays increased in stiffness by an average of 2.08 kPa per day. The effect of age on stiffness did not differ significantly among loading treatments. We also tested five setal arrays ranging in age from 881 to 894 days (approx. 2.4 years). E_{eff} averaged 30.7 kPa lower in aged arrays, yet the effect of loading direction on E_{eff} was similar to that on fresh arrays. In aged arrays, E_{eff} during vertical and +45° compression were 62±2.4 kPa and 53±2.1 kPa (mean ± s.e.m.), respectively. E_{eff} during –45° compression was 73±3.2 kPa. Mean coefficient of friction (μ) in aged arrays during the drag step was similar to that of fresh arrays; μ was 0.26±0.016 in the –45° trials, 0.24±0.016 in the +45° trials, and did not differ statistically between +45 and –45 loading directions (t=0.852; d.f.=97; P=0.39).

Discussion

Conventional adhesives are materials that are used to join two surfaces. Liquid hard-set adhesives (e.g. epoxy or

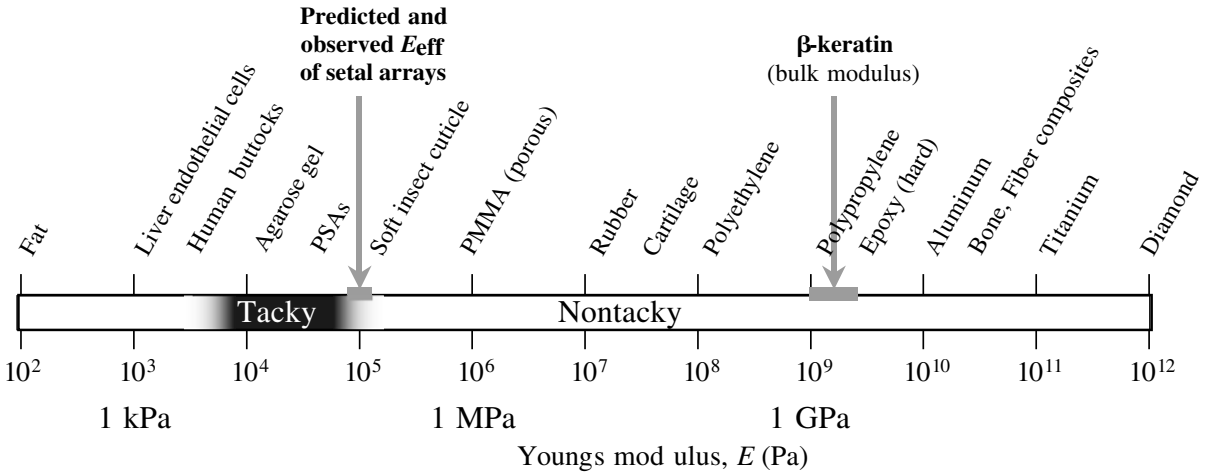

Fig. 9. Young's modulus (E) of materials including approximate values of bulk β-keratin and effective modulus (E_{eff}) of natural setal arrays (Geisler et al., 2005). A value of $E \approx 100$ kPa (measured at 1 Hz) is the upper limit of the Dahlquist criterion for tack, which is based on empirical observations of pressure sensitive adhesives [PSAs (Dahlquist, 1969; Pocius, 2002)]. A cantilever beam model [equation 5.3 (Sitti and Fearing, 2003)] predicts a value of E_{eff} near 100 kPa, as observed for natural setae and PSAs. It is notable that geckos have evolved E_{eff} close to the limit of tack. This value of E_{eff} may be tuned to allow strong and rapid adhesion, yet prevent spontaneous or inappropriate attachment.

cyanoacrylate glues) flow easily during application, but cure to make a strong, permanent bond. Because they are stiff when cured, hard-set adhesives can resist plastic creep caused by sustained loading. However, hard-set adhesives are single-use: their bonds must be broken or dissolved for removal and once broken, hard-set adhesives do not rebond. Conventional pressure sensitive adhesives (PSAs) are fabricated from soft, tacky, viscoelastic materials (Gay, 2002; Gay and Leibler, 1999; Pocius, 2002). Tacky materials are those that exhibit spontaneous plastic deformation that increases the true area of contact with the surface at the molecular scale. Theoretical considerations (Creton and Leibler, 1996) agree with Dahlquist's empirical observation (Dahlquist, 1969; Pocius, 2002) that a Young's modulus (E) below 100 kPa (at 1 Hz) is needed to achieve a high contact fraction with the substrate. PSAs such as masking tape or sticky notes are capable of repeated attachment and detachment cycles without residue because the dominant mechanism of adhesion is weak intermolecular forces. However, because they are soft polymeric materials, PSAs are prone to creep, degradation, self-adhesion and fouling.

In contrast to the soft polymers of PSAs, the adhesive on the toes of geckos is made of hard protein (β-keratin) with E 4–5 orders of magnitude greater than the upper limit of Dahlquist's criterion (Fig. 9). Therefore, one would not expect a β-keratin structure to function as a PSA by deforming readily to make intimate molecular contact with a variety of surface profiles. However, since the gecko adhesive is a microstructure in the form of an array of millions of high aspect ratio shafts (setae) the effective elastic modulus, E_{eff} (Glassmaker et al., 2004; Hui et al., 2004; Jagota and Bennison, 2002; Persson, 2003; Sitti and Fearing, 2003; Spolenak et al., 2005) is lower than E of bulk β-keratin.

The structural complexity of the setae, and their arrangement in arrays (Figs 1, 2), suggest that complex models may be needed to predict system function fully. It is advisable, however, to begin with a template model (Full and Koditschek, 1999), the simplest model (fewest number of variables and parameters) that best describes system behavior. Templates may then be grounded in more detailed (anchored) models to ask specific questions. This study suggests that the cantilever model is a good template for the behavior of setal arrays under loading and unloading conditions.

Support for the cantilever model

Highly linear forces of deformation under all loading directions support the validity of the cantilever model, and of identifying a single value of the effective modulus of the array. E_{eff} of setal arrays during vertical and +45° compression (along the natural path of drag and curvature of the setae)

The measured compliance under all loading directions supports the validity of the cantilever model. This correlation, however, appears strongest at larger displacements. As evident in Figs 6 and 7, arrays were significantly more compliant at the start of loading. We believe that this initial compliance is due to height variation in the setae, which prevent some of the setae from making initial contact and contributing to the deformation resistance. At larger displacements, complete contact is expected, leading to an effective stiffening of the array. As shown in Fig. 7, both contact regimes exhibit a linear force–displacement relationship. After initial contact, E_{eff} of setal arrays during vertical and +45° compression increased to 83±4.0 kPa and 86±4.4 kPa (mean ± s.e.m.), respectively. As predicted, the measured compliance satisfied Dahlquist's condition for tack (E_{eff}<100 kPa). Setae became significantly stiffer when compressed against the natural path of drag: E_{eff} during –45° compression was 110±4.7 kPa. Using Eqn 8, we arrive at a predicted value of 67.8 kPa for +45° compression,

20% below the observed value of 86 kPa. Eqn 8 yields a highly accurate predicted value of 113.8 kPa for –45° compression.

Additionally, we observed values of the resting angle of setal shafts (ϕ) for tokay gecko setae near 43°, consistent with the cantilever model. The difference in stiffness between fresh and aged setal arrays provided an opportunity to test the generality of the anisotropic stiffness effects we observed. Aged arrays were softer by approx. 30%, yet the forces of deformation followed a similar pattern as for fresh arrays, in which –45° compression resulted in significantly increased stiffness. The mechanism underlying the change in stiffness over time remains unknown, and merits further investigation. However, only changes over the timescale of the shed cycle of the animal (approximately 2 months) will be biologically relevant.

It is interesting to note that using the full expression in Eqn 3 for shear leads to a prediction of an effective friction coefficient that is compatible with experimental measurements. The effective friction coefficient μ_{eff} is defined as the ratio of the measured shear force to the applied compressive load. Mathematically, this may be represented as

$$\mu_{eff} = V/F = \mu + S/F . \quad (15)$$

Since the setal array is more compliant under +45° compression, a smaller load F is necessary to achieve a prescribed normal displacement. Hence, by Eqn 15, the effective friction coefficient is expected to be larger for +45° than for –45° compression. This is consistent with the values of μ of 0.24 and 0.29 measured for the –45° and +45° trials, respectively.

We conclude that, unlike synthetic PSAs, setal arrays can be modeled as Hookean elastic solids. A good template model for a setal array is a bed of springs with a directional stiffness. A linear spring rate will assist in alignment of the adhesive spatular tips with the contact surface over a wide range of displacement.

Requirements for attachment

Previously, we measured the adhesive and shear force of a single isolated gecko seta on an aluminum wire (Autumn et al., 2000). A small normal preload force, combined with a 5 μm shear displacement (proximally, along the natural path of the seta) yielded a very large shear force of 200 μN, 32× the force predicted by whole-animal measurements (Irschick et al., 1996) and 100× the frictional force measured with the seta oriented with spatulae facing away from the surface (Autumn et al., 2000). Preload and drag steps were necessary to initiate significant adhesion in isolated gecko setae, likely because mechanical deformation is needed to achieve a high contact fraction with the substrate. Autumn and Hansen estimated that only 6.6% of the area at the tip of a seta is available for initial contact with a surface when setae are in their unloaded state (Autumn and Hansen, 2006). This suggests that initially, during a gecko's foot placement, the contact fraction of the distal region of the setal array must be very low. Yet the dynamics of the foot must be sufficient to increase the contact fraction substantially to achieve the extraordinary values of adhesion and friction that have been measured in whole animals (Autumn et al., 2002; Hansen and Autumn, 2005; Irschick et al., 1996) and isolated setae (Autumn et al., 2000; Autumn et al., 2002; Hansen and Autumn, 2005). To achieve attachment the contact fraction must increase from 6% to 46%, or by approx. 7.5-fold, following preload and drag.

With the results of this study, we can now estimate the magnitude of force and deformation required to cause this increase in contact fraction. In isolated gecko setae, a 2.5 μN preload was sufficient to yield peak adhesion of between 20 μN (Autumn et al., 2000) and 40 μN (Autumn et al., 2002). (For contact with aluminum (Autumn et al., 2000) or silicon (Autumn et al., 2002), the shear term S in Eqn 3 will dominate, whereas we assume S to be negligible for contact with Teflon™

Table 1. *Stiffness and effective elastic modulus of gecko setal arrays as a function of loading and unloading direction*

	Along natural drag path and curvature (+45°)	Vertical (0°)	Against natural drag path and curvature (–45°)
Number of tokay geckos	7	7	7
Number of setal arrays	26	26	26
Number of observations	500	504	516
Array stiffness (k_{array}) (N mm^{-1})			
Loading	1.0±0.03	1.0±0.03	1.28±0.04
Unloading stiffness	0.9±0.03	1.05±0.03	1.31±0.04
Setal stiffness (k_{seta}) (N m^{-1})			
Loading	0.08±0.004	0.08±0.003	0.11±0.004
Unloading	0.08±0.003	0.09±0.003	0.11±0.004
Effective modulus (E_{eff}) (kPa)			
Loading	86±4.4	83±4.0	110±4.7
Unloading	78±3.8	89±3.8	113±4.9
Coefficient of friction (μ_{eff})	0.29±0.01	–	0.24±0.004

Values are means ± s.e.m.
Coefficient of friction values are for setal arrays sliding on PTFE. Motion protocols for loading and unloading are illustrated in Fig. 5.

in this study.] A normal displacement of 31.1 μm is required to yield 2.5 μN of preload force, given the stiffness value measured in this study (k_{seta}=0.0804 N m^{-1}; Table 1). The value of 31.1 μm represents about half the compressive range of a typical setal array in our study.

Requirements for detachment

The surprisingly large forces generated by single setae raised the question of how geckos manage to detach their feet in just 15 ms with no measurable detachment forces (Autumn et al., 2006). Increasing the angle that the setal shaft makes with the substrate to 30° causes detachment (Autumn et al., 2000). Our estimates of the setal angle in arrays in their unloaded default state was 43° in this study, suggesting that elastic energy may be stored as the setae are bent during preload, drag and adhesion. Furthermore, a resting shaft angle of 43° suggests that setae could release spontaneously if loading is relaxed sufficiently.

Effect of cantilever model parameters on system performance

The cantilever model suggests that thinner setal shafts should decrease E_{eff} and promote a greater contact fraction on rough surfaces (Campolo et al., 2003; Jagota and Bennison, 2002; Meine et al., 2004; Persson, 2003; Persson et al., 2005; Persson and Gorb, 2003; Scherge and Gorb, 2001; Sitti and Fearing, 2003; Spolenak et al., 2005; Stork, 1983). The cantilever model also suggests that longer and softer setal shafts, and a lower shaft angle ϕ will result in better adhesion on rough surfaces because these parameters will reduce E_{eff}. On a randomly rough surface, some setal shafts should be bent in compression (concave), while others will be bent in tension (convex). The total force required to pull off a setal array from a rough surface should therefore be determined by the cumulative adhesive force of all the attached spatulae, minus the sum of the forces due to elastic deformation of compressed setal shafts. Our results suggest that aged setal arrays have a lower E_{eff}, and should therefore be able to conform to rough surfaces better than stiffer, fresh arrays.

If setae mat together (Stork, 1983), it is likely that adhesive function will be compromised. Interestingly, the same parameters that promote strong adhesion on rough surfaces should also cause matting of adjacent setae (Glassmaker et al., 2004; Hui et al., 2004; Persson, 2003; Sitti and Fearing, 2003; Spolenak et al., 2005). The distance between setae and the stiffness of the shafts will determine the amount of force required to bring the tips together for matting to occur. It follows from the cantilever model that stiffer, shorter and thicker stalks will allow a greater packing density without matting. Spolenak et al. devised 'design maps' for setal adhesive structures (Spolenak et al., 2005), an approach for visualizing the parametric trade-offs needed to satisfy the rough surface and antimatting conditions while at the same time maintaining structural integrity of the material. Spolenak et al. used an estimate of E_{eff}=1 MPa for their predictions (Spolenak et al., 2005). The results of this study indicate that this value is an order of magnitude too high – at least for tokay gecko setae, which have a value of E_{eff} of approximately 100 kPa. Comparative study of setae in other geckos will be an important area of future work. It remains unknown if E_{eff} is similar in other species of gecko, *Anolis*, *Prasinohaema* and seta-bearing arthropods.

Smart adhesion at the limit of tack

There is emerging evidence that an array of gecko setae can act like a tacky, deformable material, while individual setae and spatulae retain the structural integrity of stiff protein fibers. This may enable the gecko adhesive to tolerate heavy, repeated use without creep or degradation. Indeed theoretical considerations suggest that the fibrillar structure of the gecko adhesive can be thought of as a permanent craze (Jagota and Bennison, 2002; Persson, 2003) that can raise the fracture energy relative to a solid layer of adhesive material. As with polymer crazes, setal structures under stress could store energy elastically in each seta of the array, and then as setae are pulled off, elastic energy could be dissipated internally without contributing to propagation of the crack between the adhesive and substrate (Hui et al., 2004; Jagota and Bennison, 2002; Persson, 2003). Unlike polymer crazes, setal structures may dissipate energy primarily elastically rather than plastically.

List of symbols and abbreviations

μ	friction coefficient
ϵ	strain
σ	stress
A	area
D	density
E	Young's modulus
E_{eff}	effective elastic modulus
F	load
FFT	fast Fourier transform
I	moment of inertia
k_{array}	array stiffness
k_{seta}	setal stiffness
L_0	array height
p	modulus
PSA	pressure sensitive adhesive
PTFE	polytetrafluoroethylene
R	radius
S	shear strength
SEM	scanning electron microscope
V	shear load
Δ	displacement
ϕ	angle

We thank Bob Full, Jacob Israelachvili, Kevin Kendall, Anand Jagota, Anne Peattie and Al Pocius for helpful discussions. The research was supported by DARPA N66001-03-C-8045, NSF-NIRT 0304730, DCI/NGIA HM1582-05-2022 grants, and a gift from Johnson & Johnson Dupuy-Mitek Corporation.

References

Alibardi, L. (2003). Ultrastructural autoradiographic and immunocytochemical analysis of setae formation and keratinization in the digital pads of the gecko *Hemidactylus turcicus* (Gekkonidae, Reptilia). *Tissue Cell* **35**, 288-296.

Autumn, K. (2006). Properties, principles, and parameters of the gecko adhesive system. In *Biological Adhesives* (ed. A. Smith and J. Callow), pp. 225-255. Berlin, Heidelberg: Springer-Verlag.

Autumn, K. and Hansen, W. (2006). Ultrahydrophobicity indicates a nonadhesive default state in gecko setae. *J. Comp. Physiol. A Sens. Neural Behav. Physiol.* doi: 10.1007/s00359-006-0149-y.

Autumn, K. and Peattie, A. (2002). Mechanisms of adhesion in geckos. *Integr. Comp. Biol.* **42**, 1081-1090.

Autumn, K., Liang, Y. A., Hsieh, S. T., Zesch, W., Chan, W.-P., Kenny, W. T., Fearing, R. and Full, R. J. (2000). Adhesive force of a single gecko foot-hair. *Nature* **405**, 681-685.

Autumn, K., Sitti, M., Peattie, A., Hansen, W., Sponberg, S., Liang, Y. A., Kenny, T., Fearing, R., Israelachvili, J. and Full, R. J. (2002). Evidence for van der Waals adhesion in gecko setae. *Proc. Natl. Acad. Sci. USA* **99**, 12252-12256.

Autumn, K., Hsieh, S. T., Dudek, D. M., Chen, J., Chitaphan, C. and Full, R. J. (2006). Dynamics of geckos running vertically. *J. Exp. Biol.* **209**, 260-272.

Bhushan, B. (2002). *Introduction to Tribology*. New York: John Wiley and Sons.

Bonser, R. H. C. (2000). The Young's modulus of ostrich claw keratin. *J. Mater. Sci. Lett.* **19**, 1039-1040.

Bonser, R. H. C. and Purslow, P. P. (1995). The Young's modulus of feather keratin. *J. Exp. Biol.* **198**, 1029-1033.

Campolo, D., Jones, S. D. and Fearing, R. S. (2003). Fabrication of gecko foot-hair like nano structures and adhesion to random rough surfaces. In *IEEE Nano 2003 Aug 12-14*, vol. 2, pp. 856-859. San Francisco: IEEE. doi:10.1109/NANO.2003.1231049.

Creton, C. and Leibler, L. (1996). How does tack depend on contact time and contact pressure? *J. Polym. Sci. B* **34**, 545-554.

Dahlquist, C. A. (1969). Pressure-sensitive adhesives. In *Treatise on Adhesion and Adhesives.* Vol. 2 (ed. R. L. Patrick), pp. 219-260. New York: Dekker.

Fakley, M. (2001). Smart adhesives. *Chem. Ind.* **21**, 691-695.

Fraser, R. D. B. and Parry, D. A. D. (1996). The molecular structure of reptilian keratin. *Int. J. Biol. Macromol.* **19**, 207-211.

Frisch-Fay, R. (1962). *Flexible Bars*. Washington DC: Butterworths.

Full, R. J. and Koditschek, D. E. (1999). Templates and anchors: neuromechanical hypotheses of legged locomotion on land. *J. Exp. Biol.* **202**, 3325-3332.

Gay, C. (2002). Stickiness – some fundamentals of adhesion. *Integr. Comp. Biol.* **42**, 1123-1126.

Gay, C. and Leibler, L. (1999). Theory of tackiness. *Phys. Rev. Lett.* **82**, 936-939.

Geisler, B., Dittmore, A., Gallery, B., Stratton, T., Fearing, R. and Autumn, K. (2005). Deformation of isolated gecko setal arrays: bending or buckling? 2. Kinetics. *Int. Comp. Biol.* **44**, 557.

Glassmaker, N. J., Jagota, A., Hui, C. Y. and Kim, J. (2004). Design of biomimetic fibrillar interfaces: 1. Making contact. *J. R. Soc. Interface* **1**, 1-11.

Hansen, W. and Autumn, K. (2005). Evidence for self-cleaning in gecko setae. *Proc. Natl. Acad. Sci. USA* **102**, 385-389.

Hui, C. Y., Glassmaker, N. J., Tang, T. and Jagota, A. (2004). Design of biomimetic fibrillar interfaces: 2. Mechanics of enhanced adhesion. *J. R. Soc. Interface* **1**, 12-26.

Irschick, D. J., Austin, C. C., Petren, K., Fisher, R., Losos, J. B. and Ellers, O. (1996). A comparative analysis of clinging ability among pad-bearing lizards. *Biol. J. Linn. Soc. Lond.* **59**, 21-35.

Jagota, A. and Bennison, S. (2002). Mechanics of adhesion through a fibrillar microstructure. *Integr. Comp. Biol.* **42**, 1140-1145.

Meine, K., Kloss, K., Schneider, T. and Spaltmann, D. (2004). The influence of surface roughness on the adhesion force. *Surf. Interface Anal.* **36**, 694.

Persson, B. N. J. (2003). On the mechanism of adhesion in biological systems. *J. Chem. Phys.* **118**, 7614-7621.

Persson, B. N. J. and Gorb, S. (2003). The effect of surface roughness on the adhesion of elastic plates with application to biological systems. *J. Chem. Phys.* **119**, 11437.

Persson, B. N. J., Albohr, O., Tartaglino, U., Volokitin, A. I. and Tosatti, E. (2005). On the nature of surface roughness with application to contact mechanics, sealing, rubber friction and adhesion. *J. Phys. Condens. Matter* **17**, R1-R62.

Pocius, A. V. (2002). *Adhesion and Adhesives Technology: An Introduction* (2nd edn). Munich: Hanser Verlag.

Ruibal, R. and Ernst, V. (1965). The structure of the digital setae of lizards. *J. Morphol.* **117**, 271-294.

Russell, A. P. (1975). A contribution to the functional morphology of the foot of the tokay, *Gekko gecko* (Reptilia, Gekkonidae). *J. Zool. Lond.* **176**, 437-476.

Russell, A. P. (1986). The morphological basis of weight-bearing in the scansors of the tokay gecko (Reptilia: Sauria). *Can. J. Zool.* **64**, 948-955.

Russell, A. P. (2002). Integrative functional morphology of the gekkotan adhesive system (Reptilia: Gekkota). *Integr. Comp. Biol.* **42**, 1154-1163.

Scherge, M. and Gorb, S. N. (2001). *Biological Micro- and Nanotribology: Nature's Solutions*. Berlin: Springer.

Schleich, H. H. and Kästle, W. (1986). Ultrastrukturen an gecko-zehen (Reptilia: Sauria: Gekkonidae). *Amphib. Reptil.* **7**, 141-166.

Simmermacher, G. (1884). Haftapparate bei wirbeltieren. *Zool. Garten* **25**, 289-301.

Sitti, M. and Fearing, R. S. (2003). Synthetic gecko foot-hair micro/nano structures as dry adhesives. *J. Adhesion Sci. Technol.* **17**, 1055-1073.

Spolenak, R., Gorb, S. and Arzt, E. (2005). Adhesion design maps for bio-inspired attachment systems. *Acta Biomater.* **1**, 5-13.

Stork, N. E. (1983). A comparison of the adhesive setae on the feet of lizards and arthropods. *J. Nat. Hist.* **17**, 829-835.

Tong, T., Zhao, Y., Delzeit, L., Majidi, C., Groff, R. E., Reddy, P., Majumdar, A., Kashani, A. and Meyyappan, M. (2005). Compressive properties of dense vertically aligned multi-walled carbon nanotube arrays. In *NANO2005 ASME Integrated Nanosystems: Design, Synthesis & Applications. September 14-16, 2005*. Berkeley, California, USA.

Wainwright, S. A., Biggs, W. D., Currey, J. D. and Gosline, J. M. (1982). *Mechanical Design in Organisms*. Princeton: Princeton University Press.

Williams, E. E. and Peterson, J. A. (1982). Convergent and alternative designs in the digital adhesive pads of scincid lizards. *Science* **215**, 1509-1511.